

# Molecular modelling and simulation of the surface tension of real quadrupolar fluids

Stephan Werth<sup>a</sup>, Katrin Stöbener<sup>b</sup>, Peter Klein<sup>b</sup>, Karl-Heinz Küfer<sup>b</sup>,  
Martin Horsch<sup>a,\*</sup>, Hans Hasse<sup>a</sup>

<sup>a</sup>*University of Kaiserslautern, Laboratory of Engineering Thermodynamics,  
Erwin-Schrödinger Str. 44, D-67663 Kaiserslautern, Germany*

<sup>b</sup>*Fraunhofer Institute for Industrial Mathematics, Department for Optimization,  
Fraunhofer-Platz 1, D-67663 Kaiserslautern, Germany*

---

## Abstract

Molecular modelling and simulation of the surface tension of fluids with force fields is discussed. 29 real fluids are studied, including nitrogen, oxygen, carbon dioxide, carbon monoxide, fluorine, chlorine, bromine, iodine, ethane, ethylene, acetylene, propyne, propylene, propadiene, carbon disulfide, sulfur hexafluoride, and many refrigerants. The fluids are represented by two-centre Lennard-Jones plus point quadrupole models from the literature. These models were adjusted only to experimental data of the vapour pressure and saturated liquid density so that the results for the surface tension are predictions. The deviations between the predictions and experimental data for the surface tension are of the order of 20 %. The surface tension is usually overestimated by the models. For further improvements, data on the surface tension can be included in the model development. A suitable strategy for this is multi-criteria optimization based on Pareto sets. This is

---

\*Corresponding author. E-mail: martin.horsch@mv.uni-kl.de; phone: +49 631 205 3227; fax: +49 631 205 3835.

demonstrated using the model for carbon dioxide as an example.

---

## 1. Introduction

In classical phenomenological thermodynamics following Gibbs [1], interfacial properties are considered as excess contributions which are assigned to a formal dividing surface. In this way, the surface tension is obtained from the excess free energy with respect to a hypothetical system that does not contain an interface, consisting of the bulk phases in thermodynamic equilibrium only. Theorems that hold for the bulk properties can be immediately applied to interfacial thermodynamics, yielding fundamental relations such as the Gibbs adsorption equation [1, 2].

In interfacial thermodynamics, the Gibbs dividing surface represents the highest level of abstraction. Being strictly two-dimensional, the dividing surface does not have any volume, and its internal structure is not considered. While this simplifies the theoretical framework, it neglects physical phenomena which are important for understanding fluid interfaces. Since van der Waals [3], it has been understood that such a purely empirical description can benefit from a theory of the fluid interface as a continuous region connecting two phases.

Thermodynamically, the internal structure of the interface, such as its thickness, can be considered by generalized versions of the Gibbs approach, e.g. as devised by Guggenheim [4] or from more recent work [5, 6]. Furthermore, investigations based on statistical mechanics can provide a more detailed insight by describing the thermodynamics of interfaces in terms of their molecular structure [7, 8]. In particular, density functional theory (DFT) in

24 combination with molecular equations of state was found to be a viable ap-  
25 proach for interfacial properties of pure fluids [9, 10] as well as mixtures  
26 [9, 11]. In combination with simple expressions for the free energy, DFT  
27 yields analytical results such as the well-known approximation of the density  
28 profile by a hyperbolic tangent [12].

29 Molecular dynamics (MD) simulation, on the other hand, is based on the  
30 equations of motion from classical mechanics. While it is computationally  
31 more expensive, systems containing up to trillions of molecules can today be  
32 simulated on supercomputers, employing numerically convenient pair poten-  
33 tials [13, 14]. With relatively few model parameters, which can be adjusted  
34 to experimental data, molecular pair potentials are highly reliable for extrap-  
35 olating and predicting a wide variety of fluid properties consistently [15, 16].  
36 Both static and dynamic properties can be computed by MD simulation [17–  
37 19], for bulk phases as well as for heterogeneous systems [20, 21]. Even heat  
38 and mass transfer at fluid interfaces is well accessible to molecular dynamics  
39 [22, 23].

40 In a homogeneous bulk fluid, the long-range part of the force field acting  
41 on a single molecule averages out beyond a certain cutoff radius  $r_c$ , and  
42 straightforward mean-field approximations can be applied to compute the  
43 long-range contribution to the energy and the pressure [24]. For simulations  
44 in the canonical ensemble, these corrections can be treated statically for  
45 the Lennard-Jones potential, and even for dipolar molecules [25], i.e. they  
46 have to be computed only once and do not change over time. However,  
47 molecular simulation of heterogeneous systems is more challenging, since the  
48 approximations behind the most straightforward techniques for homogeneous

49 systems, e.g. the reaction field method [26], break down in an anisotropic  
50 environment.

51 At a vapour-liquid interface, a volume integral over a short-range interac-  
52 tion such as dispersion, which decays with  $r_{ij}^{-6}$  in terms of the intermolecular  
53 distance  $r_{ij}$ , can yield a significant contribution, of the order of  $r_c^{-3}$ , to the  
54 potential energy as well as the surface tension [27]. Various algorithms have  
55 been devised to compute such effects efficiently and in a scalable way [28, 29],  
56 facilitating the massively-parallel MD simulation of heterogeneous systems  
57 with large numbers of particles [30, 31].

58 On the molecular level, the surface tension  $\gamma$  can be considered in different  
59 ways, based on mechanical and thermodynamic approaches. Thermodynam-  
60 ically, the surface tension is defined by the free energy change related to a  
61 differential variation of the surface area. Such differential excess free energies  
62 can be determined by test-area simulation [32, 33], whereas approaches based  
63 on grand-canonical sampling yield the absolute excess free energy associated  
64 with the interface [34–38].

65 Mechanically, an interfacial tension causes a local stress, i.e. a negative  
66 pressure, which acts in the direction tangential to the interface. For the  
67 vapour-liquid surface tension at curved interfaces, mechanical and thermo-  
68 dynamic methods lead to contradicting results [38–40], and thermodynamic  
69 statements cannot be based on the mechanically defined value of  $\gamma$  directly.  
70 In case of planar fluid interfaces, however, the mechanical and thermody-  
71 namic approaches are rigorously equivalent, and the mechanical approach,  
72 which is employed here, can be straightforwardly implemented in terms of  
73 the intermolecular virial [41]. If periodic boundary conditions are employed

74 and the canonical ensemble is simulated, the surface tension is immediately  
75 related to the deviation between the normal and tangential components of  
76 the pressure tensor.

77 Accurate molecular simulation results for the surface tension require an  
78 adequate consideration of the long-range contribution, which is sometimes  
79 nonetheless absent from works reporting such values [16, 42]. Molecular  
80 models for which the surface tension has recently been evaluated reliably  
81 include carbon dioxide [43, 44], which is also considered in the present work,  
82 water models [43, 45], and several other molecular fluids [46, 47]. Comparing  
83 model predictions to experimental data, deviations were found to be of the  
84 order of 10 to 20 % for various molecular models from the literature [43, 46,  
85 47] and typically of the order of 50 % for water models [45].

86 However, no systematic evaluation of  $\gamma$  by MD simulation of an entire  
87 class of molecular models has been conducted so far. This is the aim of the  
88 present work, focusing on a simple, but powerful class of models for real fluids  
89 from the literature. Vrabec et al. [48] and Stoll et al. [49] developed molecular  
90 models of the two-centre Lennard-Jones plus point quadrupole (2CLJQ) type  
91 for 29 real compounds, including air components, halogens, hydrocarbons,  
92 and refrigerants. In previous work, these models were also applied success-  
93 fully to binary [50] and ternary mixtures [51]. The vapour-liquid equilibrium  
94 (VLE) behaviour of the 2CLJQ model fluid has been studied systematically  
95 [52], serving as the basis for a molecular equation of state which contains an  
96 explicit contribution of the quadrupole moment [53].

97 A correlation for the surface tension of the 2CLJQ model fluid from pre-  
98 vious work [54] is extended by new MD simulations in the present work. On

99 this foundation, the predictive capacity regarding the surface tension of the  
100 planar vapour-liquid interface is assessed here for these models, which were  
101 adjusted to VLE properties of the bulk fluids only [48, 49], i.e. interfacial  
102 properties were not taken into account for the parametrization.

103 For the present MD simulations of the surface tension, an efficient algo-  
104 rithm is employed to compute the contribution of the long-range correction  
105 [29], combining an integration over planar slabs [27] with a centre-of-mass  
106 cutoff for multi-site models [55]. The obtained vapour-liquid surface tension  
107 is entirely predictive, and a comparison with experimental data can serve to  
108 validate or improve the molecular models. The surface tension predicted by  
109 these models has not been studied previously, except for molecular nitrogen  
110 and oxygen, where Eckelsbach et al. [47] found a deviation of about 15 %  
111 between model properties and experimental data. The present work con-  
112 firms this result and considers the whole set of 2CLJQ models of real fluids  
113 systematically.

114 The agreement of a molecular model with real fluid properties, e.g. for  
115 the surface tension, can be improved by taking the respective experimen-  
116 tal data explicitly into account when the model parameters are optimized.  
117 In the literature, various optimization approaches employing a single objec-  
118 tive function can be found [16, 64–66]. Thereby, the objective function is  
119 designed to represent the quality of several thermodynamic properties simul-  
120 taneously, and specific preferences of the model developer are expressed by  
121 setting weights for these properties. To find the minimum of the objective  
122 function, gradient based algorithms can be applied, e.g. starting from a refer-  
123 ence model from literature or based on quantum chemical calculations. The

124 derivative of the objective function over the model parameters is evaluated  
125 and the steepest descent defines the change in the parameters.

126 In the present work, a multi-criteria optimization approach is used instead  
127 to identify the Pareto set, i.e. the set of molecular models which cannot be  
128 altered without ranking worse according to at least one of the considered  
129 criteria. Here, several objective functions can be defined and optimized si-  
130 multaneously. Since different criteria generally represent conflicting goals, it  
131 is not possible to find a molecular model leading to a minimum in all objec-  
132 tive functions. Instead, the set of Pareto optimal molecular models (i.e. the  
133 Pareto set), is determined by which all possible compromises between the ob-  
134 jective functions are accessible. Knowing the Pareto set, one can choose the  
135 model best suited for a particular application. In previous work of Stöbener  
136 et al. [59], this approach was applied to the single-centre Lennard-Jones fluid,  
137 which has two model parameters. In the present work, the four-dimensional  
138 parameter space of the 2CLJQ model is explored, yielding a comprehensive  
139 description of CO<sub>2</sub> in terms of three objective functions, corresponding to  
140 three thermodynamic properties: The vapour pressure, the saturated liquid  
141 density, and the surface tension.

142 This article is structured as follows: In Section 2, the simulation method  
143 is briefly described. Simulation results on the predictive power of the 2CLJQ  
144 molecular models from the literature, regarding the surface tension, are pre-  
145 sented in Section 3. Multi-criteria optimization of molecular models is dis-  
146 cussed and applied to carbon dioxide in Section 4, leading to the conclusion  
147 in Section 5.

148 **2. Simulation Method**

149 The molecular models in the present work consist of two identical Lennard-  
 150 Jones sites and a point quadrupole in the centre of mass. The Lennard-Jones  
 151 potential is described by

$$u_{ij}^{\text{LJ}} = 4\epsilon \left[ \left( \frac{\sigma}{r_{ij}} \right)^{12} - \left( \frac{\sigma}{r_{ij}} \right)^6 \right], \quad (1)$$

152 with the size parameter  $\sigma$  and the energy parameter  $\epsilon$ . The quadrupole-  
 153 quadrupole interaction is described by

$$u_{ij}^{\text{Q}} = \frac{1}{4\pi\epsilon_0} \frac{3Q^2}{4r_{ij}^5} f(\omega), \quad (2)$$

154 where  $\epsilon_0$  is the electric constant,  $Q$  is the quadrupole moment of the  
 155 molecules, and  $f(\omega)$  is a dimensionless angle-dependent expression [56].

156 The surface tension  $\gamma$  is obtained from the difference between the normal  
 157 and tangential contributions to the virial  $\Pi_N - \Pi_T$ , which is equivalent to  
 158 the integral over the differential pressure  $p_N - p_T$

$$\gamma = \frac{1}{2A} (\Pi_N - \Pi_T) = \frac{1}{2} \int_{-\infty}^{\infty} dy (p_N - p_T), \quad (3)$$

159 where  $2A$  denotes the area of the two dividing surfaces in the simulation  
 160 volume with periodic boundary conditions [27, 57] and  $y$  is the direction  
 161 normal to the interface.

162 Further technical details of the simulation method are described in the  
 163 Appendix.

164 **3. Prediction of the surface tension of 29 real fluids by molecular**  
165 **simulation**

166 In the following the results for the surface tension as predicted by the  
167 models of Vrabec et al. [48] and Stoll et al. [49] are presented and compared to  
168 DIPPR correlations which were adjusted to experimental data (the employed  
169 model parameters are given in the Appendix). The average deviation between  
170 the DIPPR correlation and the experimental data is below 1 % for most of  
171 the fluids studied in the present work, except CO<sub>2</sub> with an average deviation  
172 of about 4 % and R115 with about 1.8 % [58].

173 Figure 1 shows the surface tension of air components as a function of  
174 the temperature. The surface tension of N<sub>2</sub>, O<sub>2</sub> and CO is overestimated by  
175 about 15 %, while for CO<sub>2</sub> that number is 26 %. The results for the surface  
176 tension of N<sub>2</sub> and O<sub>2</sub> are similar to results of Eckelsbach et al. [47].

177 [Figure 1 about here.]

178 Figure 2 shows the surface tension of some refrigerants as a function of the  
179 temperature. The surface tension is again overestimated, but the molecular  
180 models predict the different slopes of the surface tension curve well, even  
181 though the critical temperatures of R114 and R134 are only 26 K apart.

182 [Figure 2 about here.]

183 Figure 3 shows the surface tension of halogens as a function of the tem-  
184 perature. The prediction by the molecular models are about as good as in  
185 the cases discussed above except for I<sub>2</sub>. Experimental data for the surface

186 tension of  $I_2$  are only available between about 390 and 425 K, while the criti-  
187 cal point is slightly above 800 K. The extrapolation of the DIPPR correlation  
188 may be unreliable. In the temperature range where experimental data are  
189 available, the deviation between the prediction by molecular simulation and  
190 the experimental data is about 19 %, and hence in the range as observed for  
191 the other studied systems.

192 [Figure 3 about here.]

193 Figure 4 shows the surface tension of halogenated carbons. The molecular  
194 model for  $C_2F_4$  is the only model that underestimates the surface tension.

195 [Figure 4 about here.]

196 The surface tension of all other compounds investigated in the present  
197 work are shown in the Appendix.

198 All in all the surface tension of 29 real fluids was studied in the present  
199 work. The deviation between the prediction by the molecular models of  
200 Vrabec et al. [48] and Stoll et al. [49] which were not adjusted to experimental  
201 data for the surface tension is of the order of 20 %. The surface tension is  
202 overestimated by the models in most cases. Nevertheless, considering that  
203 only data for the saturated liquid density and the vapour pressure were used  
204 for the model development, this is a good agreement.

205 To increase the quality of the molecular models in terms of the surface ten-  
206 sion, they have to be reoptimized, taking the surface tension into account. A  
207 suitable way for doing this is multi-criteria optimization.

208 **4. Model Optimization**

209 In the following a multi-criteria optimization of the molecular model of  
 210 Vrabec et al. [48] for CO<sub>2</sub> is discussed. Besides the saturated liquid density  
 211 and the vapour pressure, which were already taken into account by Vrabec  
 212 et al. [48], now also the surface tension is considered.

213 Three objective functions  $g_i$ , depending on the molecular model param-  
 214 eters, are considered. Each objective function represents the relative mean  
 215 deviation for one relevant property  $O$ , i.e. the saturated liquid density, the  
 216 vapour pressure and the surface tension,

$$g_i = \delta O = \sqrt{\frac{1}{N} \sum_{j=1}^N \left( \frac{O^{\text{exp}}(T_j) - O^{\text{sim}}(T_j, \sigma, \epsilon, L, Q)}{O^{\text{exp}}(T_j)} \right)^2}, \quad (4)$$

217 where  $O^{\text{exp}}$  are properties calculated by DIPPR correlations and  $O^{\text{sim}}$  are  
 218 properties calculated by correlations to simulation data.

219 The DIPPR correlations are based on the entire set of experimental data  
 220 available for each fluid and deviate from the individual data points to a cer-  
 221 tain extent. The relative mean deviations between the simulation data and  
 222 the correlations are about 0.4 % for the saturated liquid density, about 1.8  
 223 % for the vapour pressure [52] and about 1.9 % for the surface tension [54].  
 224 The temperature values are equidistantly spaced from the triple point tem-  
 225 perature up to 95 % of the critical temperature in 5 K steps.

226 Figure 5 shows the influence of increasing one molecular model parameter  
 227 by 5 %, while the other parameters are kept constant, on the surface tension.  
 228 The base line corresponds to the model parameters from Vrabec et al. [48].  
 229 Increasing one energy parameter,  $\epsilon$  or  $Q$ , increases the surface tension value,

230 while increasing the size parameter,  $\sigma$  or  $L$ , decreases the surface tension  
231 value. The corresponding phase diagram and vapour pressure curve are  
232 shown in the Appendix.

233 [Figure 5 about here.]

234 The Pareto set is obtained by brute force sampling of the parameter space.  
235 Therefore lower and upper bounds were defined for the parameters,  $\sigma$ ,  $\epsilon$ ,  $L$ ,  
236  $Q$ , such that the whole Pareto set is found. The sampled grid is  $60 \times 60$   
237  $\times 60 \times 60$  points. Based on the correlations of Stoll et al. [52] and Werth  
238 et al. [54] the relative mean deviations between the simulation data and the  
239 experimental data are determined. The comparison of all molecular models  
240 generates the Pareto set.

241 Figure 6 shows the Pareto set in the parameter space on the left hand side  
242 and the objective space on the right hand side, represented by the deviation  
243 in the saturated liquid density, the vapour pressure and the surface tension.  
244 From Figure 6 it can be seen which parameter values correspond to an opti-  
245 mum in two objective functions. The molecular model of Vrabec et al. [48]  
246 for  $\text{CO}_2$  (upward triangle in Figure 6) is found to lie on the Pareto set. It  
247 represents a compromise which is excellent in the vapour pressure and the  
248 saturated liquid density, but poor in the surface tension (cf. Table 1). Some  
249 other compromises taken from the Pareto set are discussed in the following  
250 (parameters cf. Table 2). It is possible to find models which are good in  
251 the vapour pressure and the surface tension, but poor in the saturated liquid  
252 density (e.g. model  $\gamma - p$  designated by a circle in Figure 6) or models which  
253 are good in the saturated liquid density and the surface tension, but poor in

254 the vapour pressure (e.g. model  $\gamma - \rho$  designated by diamond in Figure 6).  
255 Contrarily to the model of Vrabec et al. [48] these choices are not attractive  
256 as they yield very high deviations for the quantity which is described poorly,  
257 cf. Table 1. Taking the model of Vrabec et al. [48] as a starting point, the  
258 knowledge of the Pareto set enables finding compromises which are distinctly  
259 better in the surface tension at some expense in the quality for the saturated  
260 liquid density and the vapour pressure, (e.g. model  $\gamma - \rho - p$  by downward  
261 triangle in Figure 6). Note that all models discussed in the present section  
262 are optimal according to the definition given by Pareto.

263 [Figure 6 about here.]

264 [Table 1 about here.]

265 [Table 2 about here.]

266 Table 2 shows the molecular model parameters for CO<sub>2</sub> which were selected  
267 from the Pareto set of the 2CLJQ model class as described above. The molec-  
268 ular model  $\gamma - \rho$  does not have a quadrupole moment and the quadrupole  
269 moments of the other models are slightly larger than the value used of Vrabec  
270 et al. [48]. Experimental data for the quadrupole moment are between 1.64  
271 and 4.87 DÅ [56]. The experimental C=O distance is 1.15 Å [68]. The de-  
272 viation between this value and  $L/2$  of the molecular models is less than 5  
273 %.

274 More detailed information on the representation of the different thermo-  
275 dynamic properties by the models discussed above is available in the Ap-  
276 pendix.

## 277 5. Conclusion

278 In the present work, the ability of molecular models to predict the surface  
279 tension of real compounds was tested. 29 models of the 2CLJQ type which  
280 were parameterized using only experimental data of the saturated liquid den-  
281 sity and the vapour pressure were used to predict the surface tension. The  
282 deviation between the prediction and the experimental data is usually of the  
283 order of 20 % and the surface tension is overestimated. These deviations are  
284 not large considering that they refer to data along almost the entire vapour  
285 pressure curve of the studied compounds. And that both the simulation re-  
286 sults and the experimental data are subject of errors which are of the order  
287 of 1 % and 5 % respectively.

288 Increasing the quality of the molecular models requires including the sur-  
289 face tension in the model optimization procedure. Here a multi-criteria op-  
290 timization using a Pareto approach was used to optimize a molecular model  
291 for CO<sub>2</sub> tailored for particular applications. The Pareto approach can be  
292 generally applied to include the surface tension in the model development.  
293 A suitable multi-criteria optimization approach, based on constructing the  
294 Pareto set for the considered model class with respect to multiple thermody-  
295 namic properties, was presented here and applied to carbon dioxide. With a  
296 compromise model selected from the Pareto set, fair agreement is obtained  
297 for vapour-liquid equilibrium properties of the bulk fluid as well as the surface  
298 tension.

299 ***Acknowledgment.*** The authors acknowledge financial support from  
300 BMBF within the SkaSim project and from DFG within the Collaborative  
301 Research Centre MICOS (SFB 926) as well as the Reinhart Kosseleck Pro-

302 gramme (grant HA 1993/15-1). They thank Doros Theodorou for his encour-  
303 agement as well as Wolfgang Eckhardt, Manfred Heilig, Maximilian Kohns,  
304 Kai Langenbach, Gábor Rutkai, and Jadran Vrabec for fruitful discussions.  
305 The present work was conducted under the auspices of the Boltzmann-Zuse  
306 Society of Computational Molecular Engineering (BZS), and the MD simula-  
307 tions were carried out on the *SuperMUC* at Leibniz-Rechenzentrum Garching  
308 within the large-scale scientific computing project pr83ri.

## 309 **Appendix**

### 310 **Simulation Details**

311 The simulations were performed with the molecular dynamics code *ls1*  
312 *MarDyn* [61] in the canonical ensemble with  $N = 16\,000$  particles. The  
313 parameters of the molecular models of Vrabec et al. [48] and Stoll et al. [49]  
314 are given in Table 3. The equation of motion was solved by a leapfrog  
315 integrator [62] with a time step of  $\Delta t = 1$  fs. The elongation of the simulation  
316 volume normal to the interface was  $80\sigma$  and the thickness of the liquid film  
317 in the centre of the simulation volume was  $40\sigma$  to account for finite size  
318 effects [63]. The elongation in the other spatial directions was at least  $20\sigma$ .

319 [Table 3 about here.]

320 The equilibration was conducted for 500 000 time steps and the produc-  
321 tion runs for 2 500 000 time steps to reduce statistical uncertainties. The  
322 statistical errors were estimated to be three times the standard deviation of  
323 five block averages, each over 500 000 time steps. The saturated densities

324 and the vapour pressure were calculated as an average over the respective  
325 phases excluding the area close to the interface.

326 The cutoff radius was set to  $5 \sigma$  and a centre-of-mass cutoff scheme was  
327 employed. The Lennard-Jones interactions were corrected with a slab-based  
328 long range correction (LRC) [29]. The quadrupole was assumed to have no  
329 preferred orientation, which yields a vanishing LRC contribution. Following  
330 Eq. (3), the surface tension was computed immediately from the deviation  
331 between the normal and tangential diagonal components of the overall pres-  
332 sure tensor for the whole system. Thereby, the tangential pressure  $p_T$  was  
333 determined by averaging over the two tangential components of the pressure  
334 tensor.

### 335 **Additional simulation results**

336 [Figure 7 about here.]

337 [Figure 8 about here.]

338 [Figure 9 about here.]

339 [Figure 10 about here.]

340 [Figure 11 about here.]

341 [Figure 12 about here.]

342 [Figure 13 about here.]

343 [Figure 14 about here.]

344 [Figure 15 about here.]

345 **References**

- 346 [1] J. W. Gibbs, *Transact. Connecticut Acad. Arts Sciences* 3 (1876) 108–  
347 248, (1878) 343–524.
- 348 [2] R. A. Alberty, *Langmuir* 11 (9) (1995) 3598–3600.
- 349 [3] J. D. van der Waals, Ph.D. thesis, Universiteit Leiden (1873).
- 350 [4] E. A. Guggenheim, *Transact. Faraday Soc.* 35 (1940) 397–412.
- 351 [5] T. Frolov, Y. Mishin, *J. Chem. Phys.* 131 (2009) 054702.
- 352 [6] B. B. Laird, R. Davidchack, *J. Chem. Phys.* 132 (2010) 204101.
- 353 [7] D. Henderson, F. F. Abraham, J. A. Barker, *Mol. Phys.* 31 (4) (1976)  
354 1291–1295.
- 355 [8] M. Xu, C. Zhang, Z. Du, J. Mi, *J. Phys. Chem. B* 112 (22) (2012)  
356 6514–6521.
- 357 [9] S. Jain, A. Dominik, W. G. Chapman, *J. Chem. Phys.* 127 (2007)  
358 244904.
- 359 [10] J. Gross, *J. Chem. Phys.* 131 (2009) 204705.
- 360 [11] H. Kahl, S. Enders, *Phys. Chem. Chem. Phys.* 4 (6) (2002) 931–936.
- 361 [12] B. U. Felderhof, *Physica* 48 (4) (1970) 541–560.
- 362 [13] T. C. Germann, K. Kadau, *Int. J. Mod. Phys. C* 19 (9) (2008) 1315–  
363 1319.

- 364 [14] W. Eckhardt, A. Heinecke, R. Bader, M. Brehm, N. Hammer, H. Hu-  
365 ber, H.-G. Kleinhenz, J. Vrabec, H. Hasse, M. Horsch, M. Bernreuther,  
366 C. W. Glass, C. Niethammer, A. Bode, J. Bungartz, in: Supercomput-  
367 ing (Proc. 28th ISC), no. 7905 in LNCS, Springer, Heidelberg, 2013, pp.  
368 1–12.
- 369 [15] P. Ungerer, C. Nieto Draghi, B. Rousseau, G. Ahunbay, V. Lachet, J.  
370 Mol. Liq. 134 (2007) 71–89.
- 371 [16] B. Eckl, J. Vrabec, H. Hasse, Fluid Phase Equilib. 274 (1–2) (2008)  
372 16–26.
- 373 [17] S. K. Bhatia, D. Nicholson, Phys. Rev. Lett. 90 (2003) 016105.
- 374 [18] R. J. Allen, C. Valeriani, P. R. ten Wolde, J. Phys.: Cond. Mat. 21 (46)  
375 (2009) 463102.
- 376 [19] G. Guevara Carrión, H. Hasse, J. Vrabec, in: Multiscale Molecular  
377 Methods in Applied Chemistry, no. 307 in Topics in Current Chemistry,  
378 Springer, Heidelberg, 2012, pp. 201–249.
- 379 [20] J. Vrabec, G. K. Kedia, G. Fuchs, H. Hasse, Mol. Phys. 104 (9) (2006)  
380 1509–1527.
- 381 [21] E. A. Müller, Cur. Opin. Chem. Eng. 2 (2013) 223–228.
- 382 [22] G. Strotos, M. Gavaises, A. Theodorakakos, G. Bergeles, Int. J. Heat  
383 Mass Transfer 51 (2008) 1516–1529.
- 384 [23] A. Lotfi, J. Vrabec, J. Fischer, Int. J. Heat Mass Transf. 73 (2014) 303–  
385 317.

- 386 [24] M. P. Allen, D. J. Tildesley, *Computer Simulation of Liquids*, Clarendon,  
387 Oxford, 1987.
- 388 [25] B. Saager, J. Fischer, M. Neumann, *Mol. Sim.* 6 (1) (1991) 27–49.
- 389 [26] L. Onsager, *J. Am. Chem. Soc.* 58 (8) (1936) 1486–1493.
- 390 [27] J. Janeček, *J. Phys. Chem. B* 110 (12) (2006) 6264–6269.
- 391 [28] D. Taveling, P. Springer, P. Bientinesi, A. E. Ismail, *J. Chem. Phys.*  
392 140 (2014) 024105.
- 393 [29] S. Werth, G. Rutkai, J. Vrabc, M. Horsch, H. Hasse, *Mol. Phys.*, DOI:  
394 10.1080/00268976.2013.861086 (2014).
- 395 [30] A. Arnold, F. Fahrenberger, C. Holm, O. Lenz, M. Bolten, H. Dachsels,  
396 R. Halver, I. Kabadshow, F. Gähler, F. Heber, J. Iseringhausen, M.  
397 Hofmann, M. Pippig, D. Potts, G. Sutmann, *Phys. Rev. E* 88 (2013)  
398 063308.
- 399 [31] R. Isele-Holder, W. Mitchell, J. R. Hammond, A. Kohlmeyer, A. E.  
400 Ismail, *J. Chem. Theory Comput.* 9 (12) (2013) 5412–5420.
- 401 [32] G. J. Gloor, G. Jackson, F. J. Blas, E. de Miguel, *J. Chem. Phys.* 123  
402 (2005) 134703.
- 403 [33] A. Ghoufi, P. Malfreyt, *J. Chem. Phys.* 136 (2012) 024104.
- 404 [34] K. Binder, *Z. Phys. B* 43 (1981) 119–140.
- 405 [35] K. Binder, *Phys. Rev. A* 25 (3) (1982) 1699–1709.

- 406 [36] M. Schrader, P. Virnau, D. Winter, T. Zykova-Timan, K. Binder, Eur.  
407 Phys. J. Spec. Top. 117 (1) (2009) 103–127.
- 408 [37] S. K. Das, K. Binder, Phys. Rev. Lett. 107 (2011) 235702.
- 409 [38] A. Tröster, M. Oettel, B. Block, P. Virnau, K. Binder, J. Chem. Phys.  
410 136 (2012) 064709.
- 411 [39] J. G. Sampayo, A. Malijevský, E. A. Müller, E. de Miguel, G. Jackson,  
412 J. Chem. Phys. 132 (2010) 141101.
- 413 [40] A. Malijevský, G. Jackson, J. Phys.: Cond. Mat. 24 (2012) 464121.
- 414 [41] E. Salomons, M. Mareschal, J. Phys.: Cond. Mat. 3 (20) (1991) 3645–  
415 3661.
- 416 [42] S. Braun, A. R. Imre, T. Kraska, J. Chem. Phys. 138 (2013) 244710.
- 417 [43] A. Ghoufi, F. Goujon, V. Lachet, P. Malfreyt, J. Chem. Phys. 128 (2008)  
418 154716.
- 419 [44] T. Kraska, F. Römer, A. Imre, J. Phys. Chem. B 113 (14) (2009) 4688–  
420 4697.
- 421 [45] C. Vega, E. de Miguel, J. Chem. Phys. 126 (2007) 154707.
- 422 [46] J.-C. Neyt, A. Wender, V. Lachet, P. Malfreyt, J. Phys. Chem. B 115  
423 (30) (2011) 9421–9430.
- 424 [47] S. Eckelsbach, S. K. Miroshnichenko, G. Rutkai, J. Vrabec, in: W. E.  
425 Nagel, D. H. Kröner, M. M. Resch (Eds.), High Performance Computing  
426 in Science and Engineering '13, Springer, Chur, 2014, pp. 635–646.

- 427 [48] J. Vrabec, J. Stoll, H. Hasse, *J. Phys. Chem. B* 105 (48) (2001) 12126–  
428 12133.
- 429 [49] J. Stoll, J. Vrabec, H. Hasse, *J. Chem. Phys.* 119 (21) (2003) 11396–  
430 11407.
- 431 [50] J. Vrabec, Y.-L. Huang, H. Hasse, *Fluid Phase Equilib.* 279 (2) (2009)  
432 120–135.
- 433 [51] Y.-L. Huang, J. Vrabec, H. Hasse, *Fluid Phase Equilib.* 287 (1) (2009)  
434 62–69.
- 435 [52] J. Stoll, J. Vrabec, H. Hasse, J. Fischer, *Fluid Phase Equilib.* 179 (1–2)  
436 (2001) 339–362.
- 437 [53] J. Gross, *AIChE J.* 51 (9) (2005) 2556–2568.
- 438 [54] S. Werth, M. Horsch, H. Hasse, submitted (2014).
- 439 [55] R. Lustig, *Mol. Phys.* 65 (1) (1988) 175–179.
- 440 [56] C. G. Gray, K. E. Gubbins, *Theory of Molecular Fluids, Vol. 1: Funda-*  
441 *mentals*, Clarendon, Oxford, 1984.
- 442 [57] J. P. R. B. Walton, D. J. Tildesley, J. S. Rowlinson, J. R. Henderson,  
443 *Mol. Phys.* 48 (6) (1983) 1357–1368.
- 444 [58] R. L. Rowley, W. V. Wilding, J. L. Oscarson, Y. Yang, N. A. Zundel,  
445 T. E. Daubert, R. P. Danner, *DIPPR Information and Data Evaluation*  
446 *Manager for the Design Institute for Physical Properties*, AIChE, 2013,  
447 version 7.0.0.

- 448 [59] K. Stöbener, P. Klein, S. Reiser, M. Horsch, K.-H. Küfer, H. Hasse,  
449 Fluid Phase Equilib. 373 (2014) 100–108.
- 450 [60] T. Merker, J. Vrabec, H. Hasse, Soft Mater. 10 (2012) 3–24.
- 451 [61] C. Niethammer, S. Becker, M. F. Bernreuther, M. Buchholz, W. Eck-  
452 hardt, A. Heinecke, S. Werth, H.-J. Bungartz, C. W. Glass, H. Hasse,  
453 J. Vrabec, M. Horsch, J. Chem. Theory Comput., submitted (2014).
- 454 [62] D. Fincham, Mol. Phys. 8 (3–5) (1992) 165–178.
- 455 [63] S. Werth, S. V. Lishchuk, M. Horsch, H. Hasse, Physica A 392 (10)  
456 (2013) 2359–2367.
- 457 [64] M. Hülsmann, J. Vrabec, A. Maaß, D. Reith, Comp. Phys. Comm.  
458 181 (5) (2010) 887–905.
- 459 [65] M. Hülsmann, T. Köddermann, J. Vrabec, D. Reith, Comp. Phys.  
460 Comm. 181 (3) (2010) 499–513.
- 461 [66] S. Deublein, P. Metzler, J. Vrabec, H. Hasse, Mol. Sim. 39 (2) (2012)  
462 109–118.
- 463 [67] R. Span, W. Wagner, J. Phys. Chem. Ref. Data 25 (6) (1996) 1509–1596.
- 464 [68] Landolt-Börnstein, Zahlenwerte und Funktionen aus Physik, Chemie,  
465 Astronomie, Geophysik und Technik Bd. I, Teil 2, 6. Aufl., Springer,  
466 Berlin, 1961.

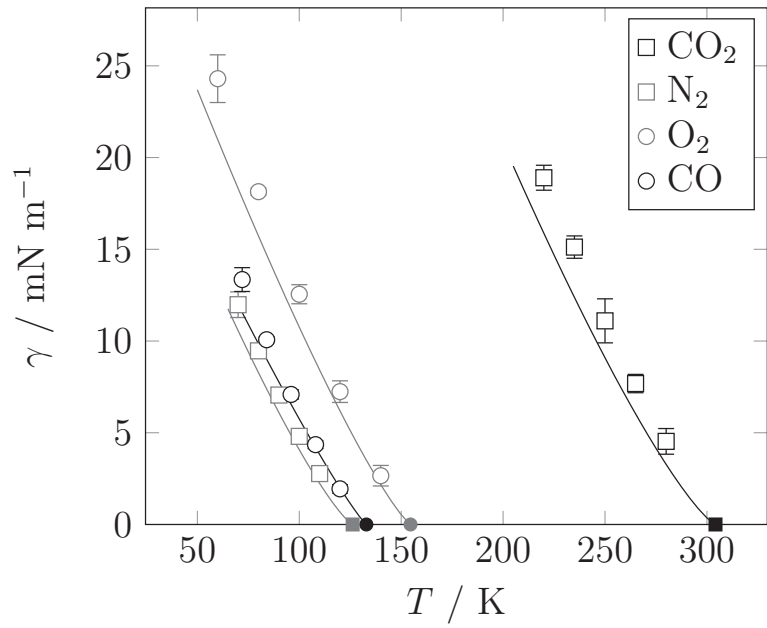


Figure 1: Surface tension of air components as a function of the temperature. The open symbols are simulation results from the present work. The solid lines represent DIPPR correlations [58], based on experimental data, and the filled symbols denote the respective critical point.

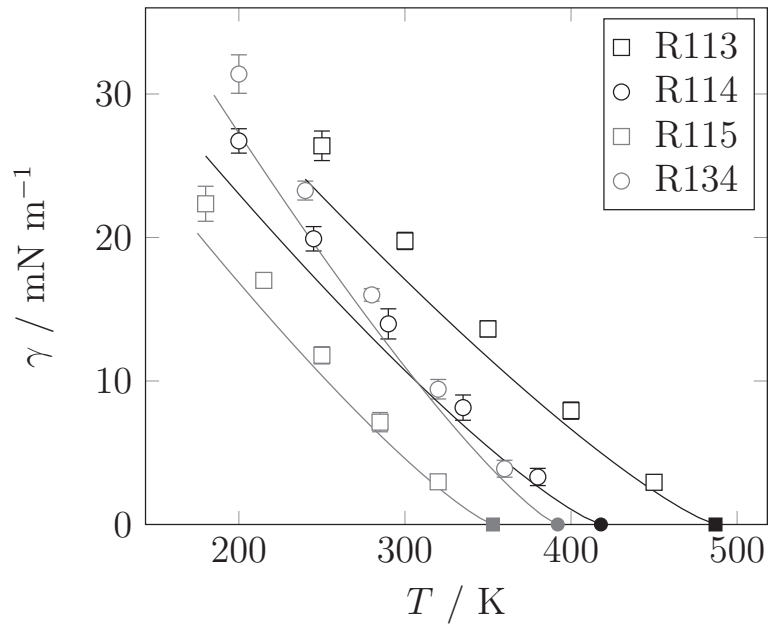


Figure 2: Surface tension of various refrigerants as a function of the temperature. The open symbols are simulation results from the present work. The solid lines represent DIPPR correlations [58], based on experimental data, and the filled symbols denote the respective critical point.

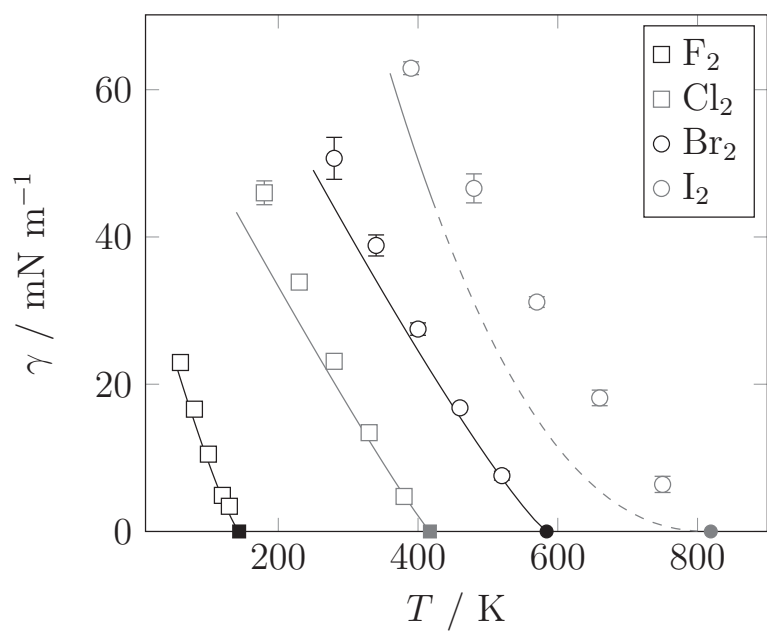


Figure 3: Surface tension of halogens as a function of the temperature. The open symbols are simulation results from the present work. The solid lines represent DIPPR correlations [58], based on experimental data, and the filled symbols denote the respective critical point. The dashed line for  $\text{I}_2$  indicates that experimental data are only available up to 425 K.

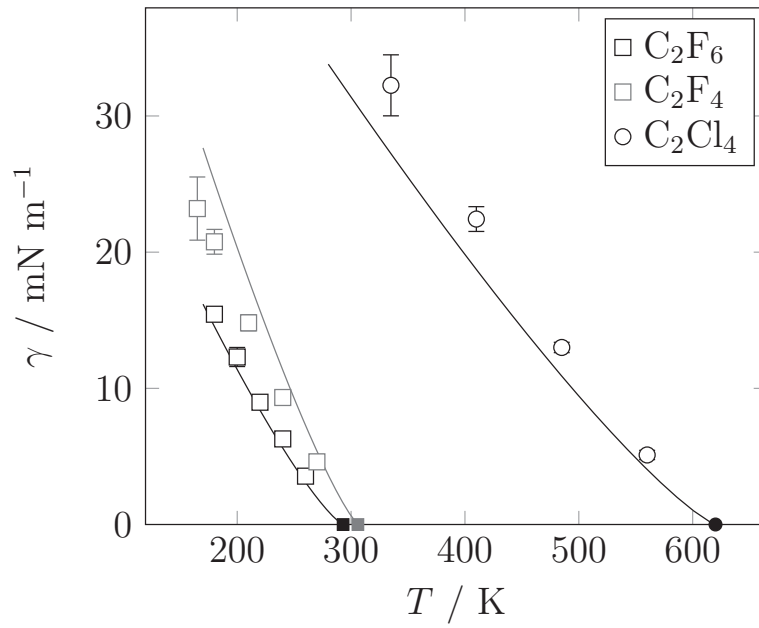


Figure 4: Surface tension of halogenated carbons as a function of the temperature. The open symbols are simulation results from the present work. The solid lines represent DIPPR correlations [58], based on experimental data, and the filled symbols denote the respective critical point.

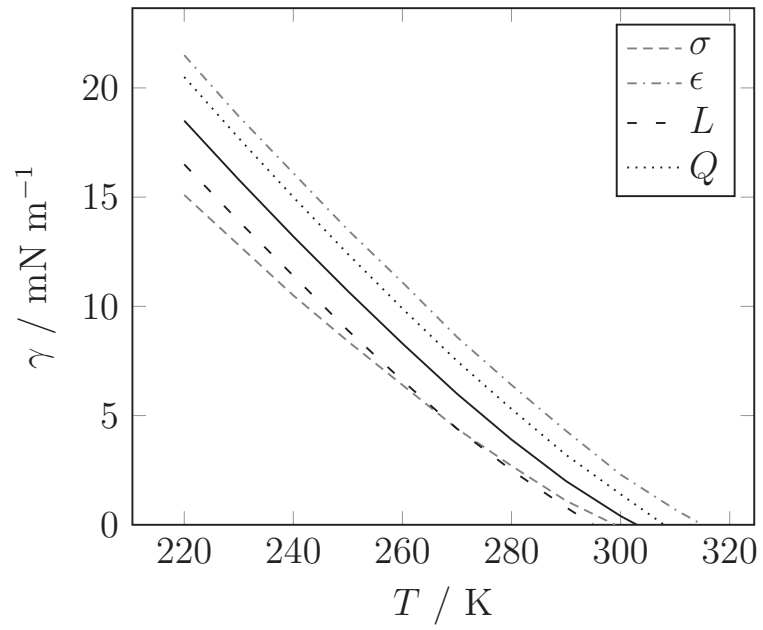


Figure 5: Surface tension of  $\text{CO}_2$ . The solid line is the base line, representing the molecular model of Vrabc et al. [48]. The dotted and dashed lines show the effect of an increase of 5 % in the corresponding model parameter.

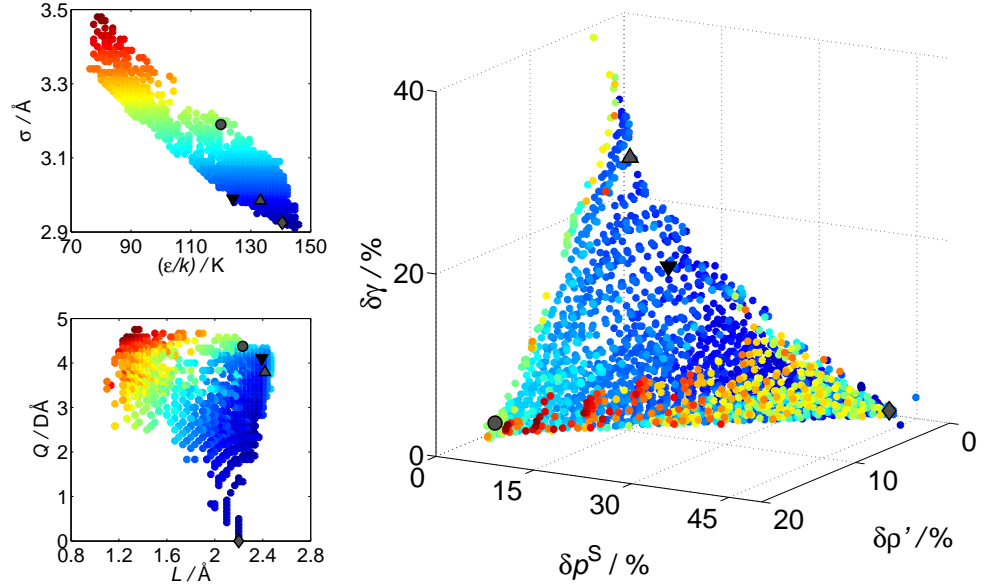


Figure 6: Pareto set of the 2CLJQ molecular models for  $\text{CO}_2$  in the parameter space, represented by the Lennard-Jones parameters  $\sigma$  and  $\epsilon$  (left top) and the model parameters  $Q$  and  $L$  (left bottom), and the objective space (right): deviations in the surface tension, the saturated density and the vapour pressure. The upward triangle denotes the molecular model of Vrabec et al. [48], the circle ( $\gamma - p$ ) and the diamond ( $\gamma - \rho$ ) denote the optimizations in two objective functions and the downward triangle denotes the new optimized molecular model ( $\gamma - \rho - p$ ). The colors represent the numerical value of  $\sigma$  and connect the points in the parameter and the objective space.

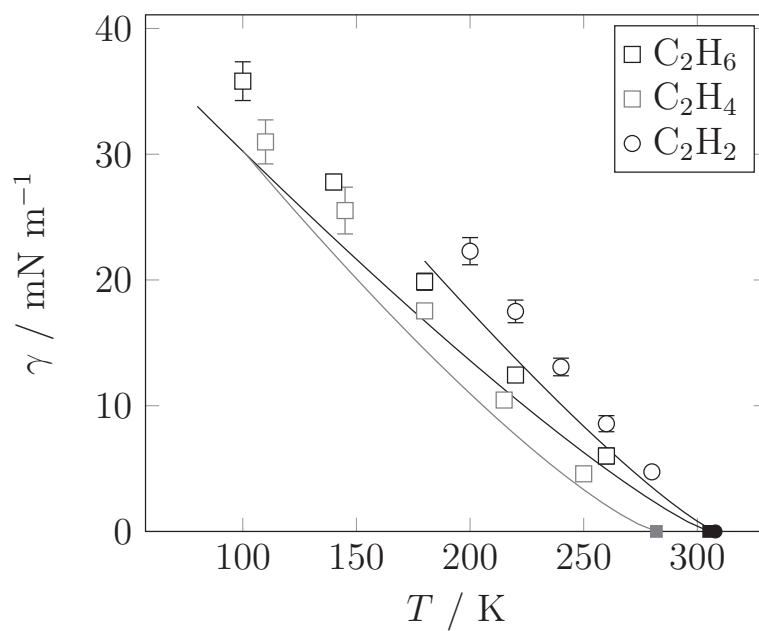


Figure 7: Surface tension of hydrocarbons as a function of the temperature. The open symbols are simulation results from the present work. The solid lines represent DIPPR correlations [58], based on experimental data, and the filled symbols denote the respective critical point.

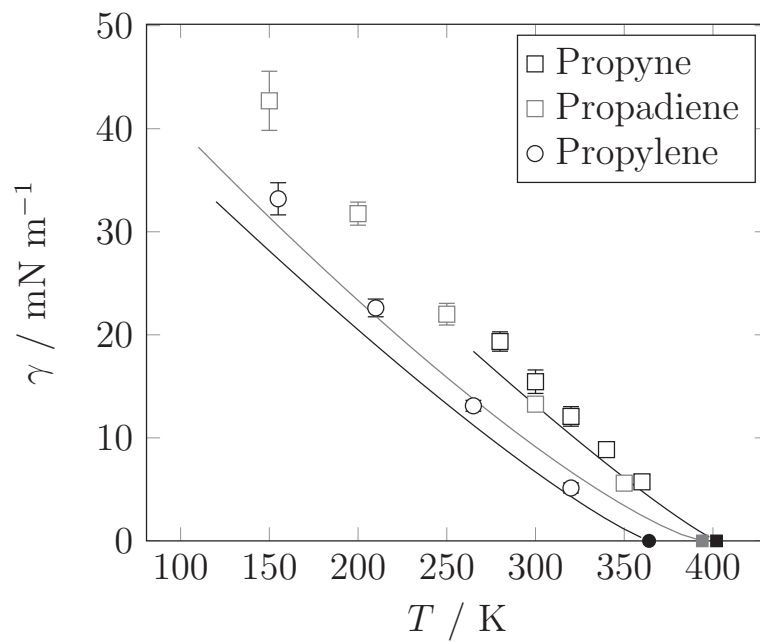


Figure 8: Surface tension of hydrocarbons as a function of the temperature. The open symbols are simulation results from the present work. The solid lines represent DIPPR correlations [58], based on experimental data, and the filled symbols denote the respective critical point.

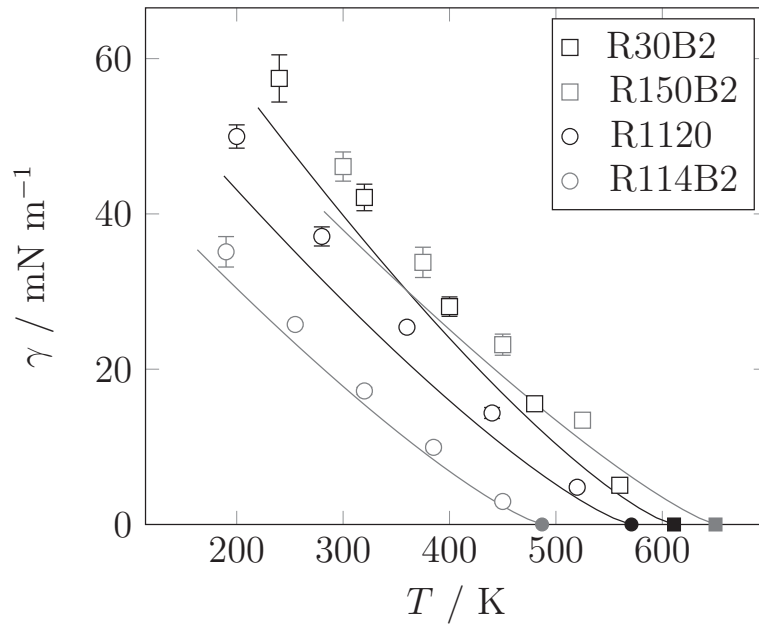


Figure 9: Surface tension of refrigerants as a function of the temperature. The open symbols are simulation results from the present work. The solid lines represent DIPPR correlations [58], based on experimental data, and the filled symbols denote the respective critical point.

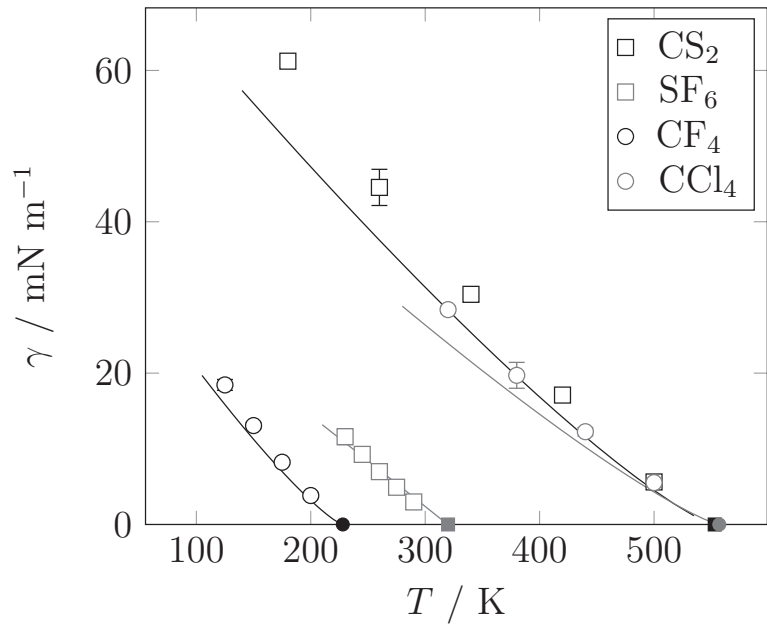


Figure 10: Surface tension of various fluids as a function of the temperature. The open symbols are simulation results from the present work. The solid lines represent DIPPR correlations [58], based on experimental data, and the filled symbols denote the respective critical point.

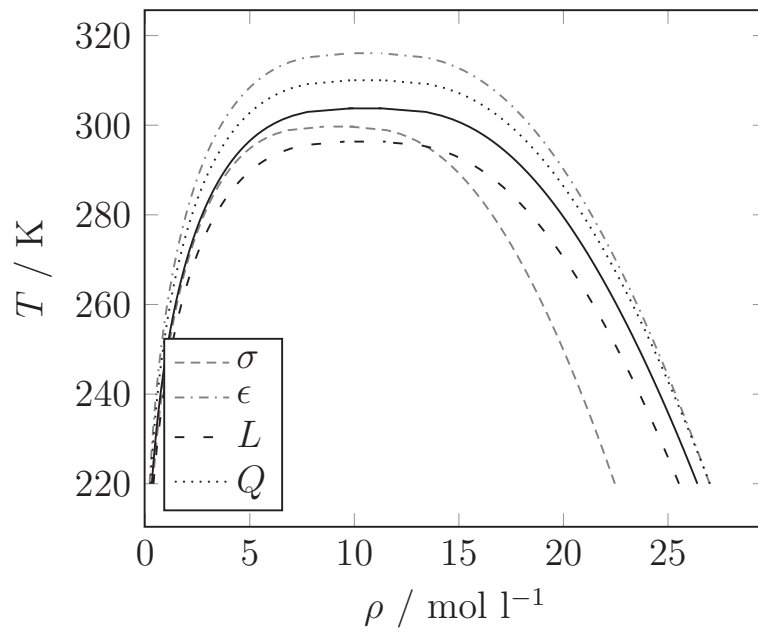


Figure 11: Saturated densities of  $\text{CO}_2$ . The solid line is the base line, representing the molecular model of Vrabc et al. [48]. The dotted and dashed lines show the effect of an increase of 5 % in the corresponding model parameter.

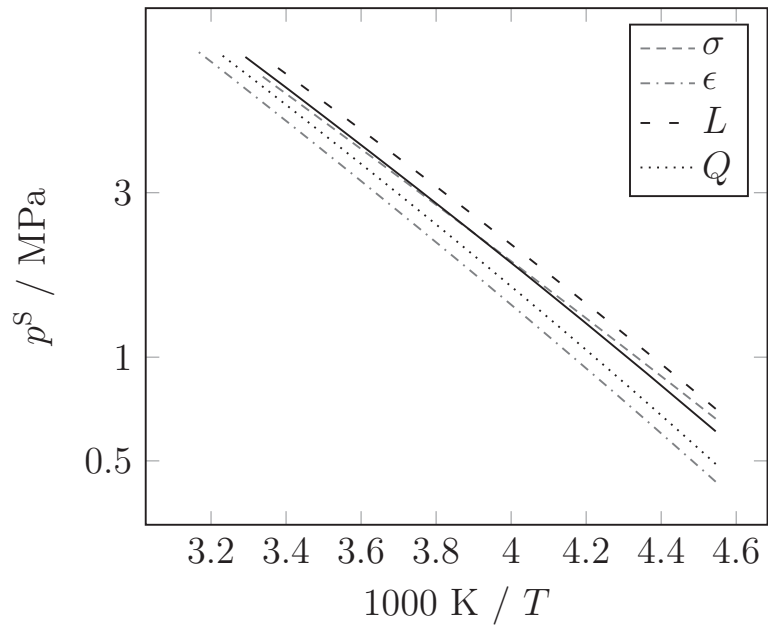


Figure 12: Vapour pressure of  $\text{CO}_2$ . The solid line is the base line, representing the molecular model of Vrabcic et al. [48]. The dotted and dashed lines show the effect of an increase of 5 % in the corresponding model parameter.

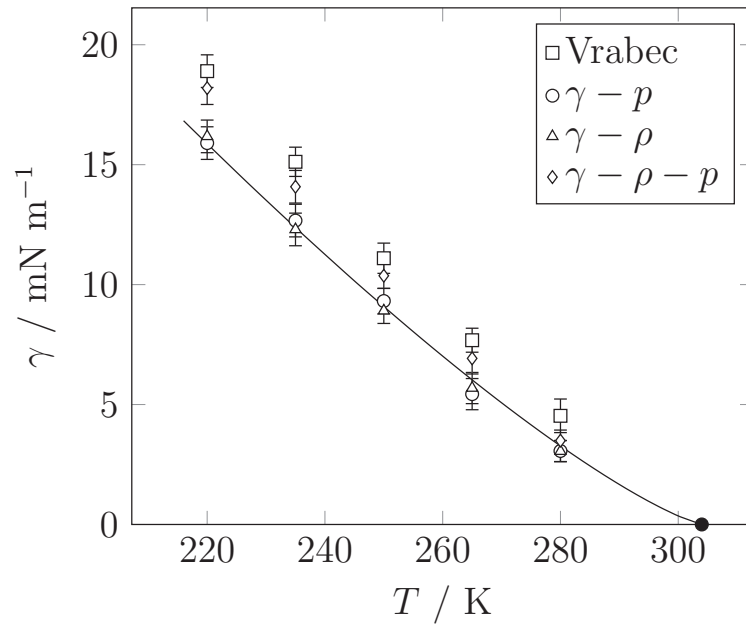


Figure 13: Surface tension of  $\text{CO}_2$  as a function of the temperature. Comparison between molecular models optimized to the surface tension and the vapour-pressure ( $\gamma - p$ ), the surface tension and the saturated liquid density ( $\gamma - \rho$ ), the optimized model ( $\gamma - \rho - p$ ) and a previous model of Vrabec et al. [48], cf. Table 2. The solid line represents the DIPPR correlation [58], based on experimental data, and the filled symbol denotes the critical point.

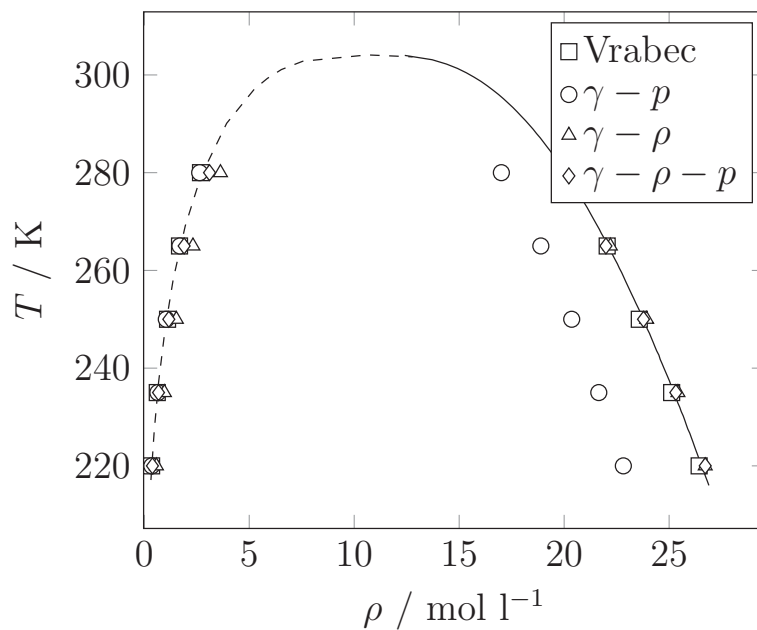


Figure 14: Saturated densities of  $\text{CO}_2$ . Comparison between molecular models optimized to the surface tension and the vapour-pressure ( $\gamma-p$ ), the surface tension and the saturated liquid density ( $\gamma-\rho$ ), the optimized model ( $\gamma-\rho-p$ ) and a previous model of Vrabc et al. [48], cf. Table 2. The solid line represents the DIPPR correlation [58], based on experimental data, the dashed line is based on an equation of state [67]. Error bars are within symbol size.

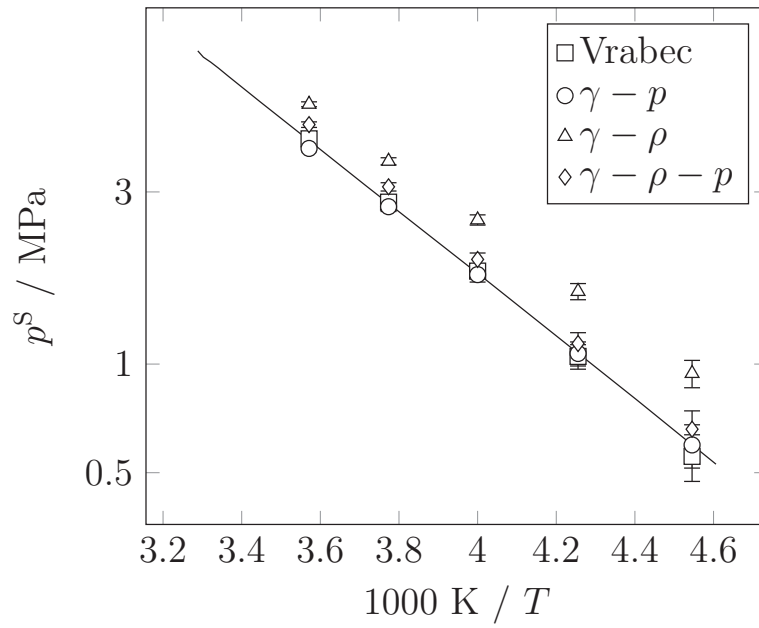


Figure 15: Vapour pressure of CO<sub>2</sub> as a function of the temperature. Comparison between molecular models optimized to the surface tension and the vapour-pressure ( $\gamma - p$ ), the surface tension and the saturated liquid density ( $\gamma - \rho$ ), the optimized model ( $\gamma - \rho - p$ ) and a previous model of Vrabec et al. [48], cf. Table 2. The solid line represents the DIPPR correlation [58], based on experimental data.

Table 1: Relative mean deviation in the saturated liquid density, the vapour pressure and the surface tension of the molecular models for CO<sub>2</sub> from Vrabec et al. [48] and the optimized versions from the present work.

	$\delta\rho' / \%$	$\delta p / \%$	$\delta\gamma / \%$
Vrabec et al. [48]	0.36	3.68	26.4
$\gamma - p$	14.4	2.60	5.42
$\gamma - \rho$	0.77	41.6	4.21
$\gamma - \rho - p$	0.86	9.24	12.3

Table 2: Parameters of the molecular models for CO<sub>2</sub> from Vrabec et al. [48] and the optimized versions from the present work.

	$\sigma / \text{\AA}$	$\epsilon / k_{\text{B}}$	$L / \text{\AA}$	$Q / \text{D}\text{\AA}$
Vrabec et al. [48]	2.9847	133.22	2.4176	3.7938
$\gamma - p$	3.19	120	2.233	4.3766
$\gamma - \rho$	2.925	140.5	2.144	-
$\gamma - \rho - p$	2.99	124	2.392	4.1091

Table 3: Parameters of the molecular models of Vrabec et al. [48] and Stoll et al. [49].

Name	Formula	CAS RN	$\sigma / \text{\AA}$	$\epsilon / k_B$	$L / \text{\AA}$	$Q / \text{D}\text{\AA}$	Author
Fluorine	$\text{F}_2$	7782-41-4	2.8258	52.147	1.4129	0.8920	[48]
Chlorine	$\text{Cl}_2$	7782-50-5	3.4016	160.86	1.9819	4.2356	[48]
Bromine	$\text{Br}_2$	7726-95-6	3.5546	236.76	2.1777	4.8954	[48]
Iodine	$\text{I}_2$	7553-56-2	3.7200	371.47	2.6784	5.6556	[48]
Nitrogen	$\text{N}_2$	7727-37-9	3.3211	34.897	1.0464	1.4397	[48]
Oxygen	$\text{O}_2$	7782-44-7	3.1062	43.183	0.9699	0.8081	[48]
Carbon dioxide	$\text{CO}_2$	124-38-9	2.9847	133.22	2.4176	3.7938	[48]
Carbon disulfide	$\text{CS}_2$	75-15-0	3.6140	257.68	2.6809	3.8997	[48]
Ethane	$\text{C}_2\text{H}_6$	74-84-0	3.4896	136.99	2.3762	0.8277	[48]
Ethylene	$\text{C}_2\text{H}_4$	74-85-1	3.7607	76.950	1.2695	4.3310	[48]
Acetylene	$\text{C}_2\text{H}_2$	74-86-2	3.5742	79.890	1.2998	5.0730	[48]
R116	$\text{C}_2\text{F}_6$	76-16-4	4.1282	110.19	2.7246	8.4943	[48]
R1114	$\text{C}_2\text{F}_4$	116-14-3	3.8611	106.32	2.2394	7.0332	[48]
R1110	$\text{C}_2\text{Cl}_4$	127-18-4	4.6758	211.11	2.6520	16.143	[48]
Propadiene	$\text{C}_3\text{H}_4$	463-49-0	3.6367	170.52	2.4958	5.1637	[48]
Propyne	$\text{C}_3\text{H}_4$	74-99-7	3.5460	186.43	2.8368	5.7548	[48]
Propylene	$\text{C}_3\text{H}_6$	115-07-1	3.8169	150.78	2.5014	5.9387	[48]
R846	$\text{SF}_6$	2551-62-4	3.9615	118.98	2.6375	8.0066	[48]
R14	$\text{CF}_4$	75-73-0	3.8812	59.235	1.3901	5.1763	[48]
R10	$\text{CCl}_4$	56-23-5	4.8471	142.14	1.6946	14.346	[48]
Carbon monoxide	$\text{CO}$	630-08-0	3.3344	36.713	1.1110	1.9170	[49]
R113	$\text{CFCl}_2\text{-CF}_2\text{Cl}$	76-13-1	4.5207	217.08	3.6166	12.984	[49]
R114	$\text{CBrF}_2\text{-CBrF}_2$	76-14-2	4.3772	183.26	3.5018	11.456	[49]
R115	$\text{CF}_3\text{-CF}_2\text{Cl}$	76-15-3	4.1891	155.77	3.3513	9.2246	[49]
R134	$\text{CHF}_2\text{-CHF}_2$	359-35-3	3.7848	170.46	3.0278	7.8745	[49]
R30B2	$\text{CH}_2\text{Br}_2$	74-95-3	3.8683	274.97	3.0946	9.2682	[49]
R150B2	$\text{CH}_2\text{Br-CH}_2\text{Br}$	106-93-4	4.1699	302.33	3.3359	10.903	[49]
R114B2	$\text{CBrF}_2\text{-CBrF}_2$	124-73-2	4.5193	218.40	3.6154	12.822	[49]
R1120	$\text{CHCl=CCl}_2$	79-01-6	4.4120	201.03	2.6357	13.624	[49]